Effects of high-power laser irradiation on sub-superficial graphitic
layers in single-crystal diamond

(Article begins on next page)

25 November 2024

1

2 **Effects of high-power laser irradiation on sub-superficial graphitic layers in single-crystal**

3 **diamond**

4

5 F. Picollo[1,2,3*], S. Rubanov[4], C. Tomba[5,6,7], A. Battiato[2,1,3], E. Enrico[8], A. Perrat-Mabilon[9,10],

6 C. Peaucelle[9,10], T. N. Tran Thi [5,9,11], L. Boarino[8], E. Gheeraert[5,7], P. Olivero[2,1,3,8]

7

8

9 *[1] National Institute of Nuclear Physics (INFN), section of Torino, Italy*

10 *[2] Physics Department and "NIS" Inter-departmental centre, University of Torino, Torino, Italy*

11 *[3] National Interuniversity Consortium for the Physical Sciences of Matter (CNISM), Torino Unit, Italy*

12 *[4] Bio21 Institute, University of Melbourne, Australia*

13 *[5] University of Grenoble Alpes, F-38000 Grenoble, France*

14 *[6] Laboratoire des Technologies de la Microelectronique, Minatec Campus, F-38054 Grenoble, France*

15 *[7] CNRS, Institute NEEL, F-38042 Grenoble, France*

16 *[8] National Institute of Metrologic Research (INRiM), Torino, Italy*

17 *[9] University of Lyon 1, CNRS, Inst Phys Nucl Lyon, F-69622 Villeurbanne, France*

18 *[10] IN2P3, F-69622 Villeurbanne, France*

19 *[11] European Synchrotron Radiation Facility (ESRF), Grenoble, France*

20 **Abstract**

21 We report on the structural modifications induced by a $\lambda = 532$ nm ns-pulsed high-power laser

22 on sub-superficial graphitic layers in single-crystal diamond realized by means of MeV ion

23 implantation. A systematic characterization of the structures obtained under different laser

24 irradiation conditions (power density, number of pulses) and subsequent thermal annealing was

25 performed by different electron microscopy techniques. The main feature observed after laser

26  irradiation is the thickening of the pre-existing graphitic layer. Cross-sectional SEM imaging was

27  performed to directly measure the thickness of the modified layers, and subsequent selective

28  etching of the buried layers was employed to both assess their graphitic nature and enhance the

29  SEM imaging contrast. In particular, it was found that for optimal irradiation parameters the laser

30  processing induces a six-fold increase the thickness of sub-superficial graphitic layers without

31  inducing mechanical failures in the surrounding crystal. TEM microscopy and EELS

32  spectroscopy allowed a detailed analysis of the internal structure of the laser-irradiated layers,

33  highlighting the presence of different nano-graphitic and amorphous layers. The obtained results

34  demonstrate the effectiveness and versatility of high-power laser irradiation for an accurate

35  tuning of the geometrical and structural features of graphitic structures embedded in

36  single-crystal diamond, and open new opportunities in diamond fabrication.

37

38

39

40  * corresponding author:     picollo@to.infn.it

41                             ph: +39 011 670 7879

42                             fax: +39 011 670 7020

43

49

## 1. Introduction

Diamond is well known for its range of extreme mechanical, thermal and optical properties, which make it an attractive material for a variety of applications [1]. Nevertheless, diamond is a metastable allotropic form of carbon at standard pressure and temperature, and can be converted into graphite if an energy barrier is overcome [2]. Several approaches have been developed to induce this phase transition, among which ion-beam-induced graphitization [3–9] and laser-induced graphitization [10,11] play a prominent role. The former approach takes advantage of the ion-induced defect creation caused by nuclear collisions to amorphize the material and the subsequent thermal annealing to convert amorphized regions into a graphitic phase [3]. The latter approach is based on complex non-equilibrium dynamics induced by high-power light absorption, which were modelled with different theoretical approaches based on the non-radiative recombination of electron-hole pairs [11] or on a non-thermal ultrafast non-equilibrium phase transition [12,13].

Several previous studies explored the laser-induced graphitization process of single-crystal diamond: the first investigations dating back to the 80's were focused on realization of graphitic structures on diamond surface with direct writing or optical projection by means of excimer lasers [14], approached that was further investigated also in recent years [15]. Subsequently, new theoretical models of pulsed laser irradiation were proposed taking into account fast energy transfer mechanisms [16]. Consequently, in the last decade several works were carried out to exploit the possibility of realizing three-dimensional structures into diamond bulk by means of femtosecond [17,18] and picosecond [18–20] pulsed laser writing. Furthermore, the possibility of enhancing the resolution in the laser fabrication of the graphitic structures with the use of adaptive optical elements was recently demonstrated [21,22].

73  Direct laser-induced graphitization represents an extremely versatile technique with promising

74  applications in different fields such as the realization of diamond-based particle detectors [23–

75  27] and (upon the selective removal of the graphite) microfluidics devices for biomedical sensing

76  [28].

77  On the other hand, this technique is limited by the poor geometrical quality of structures

78  finishing, which is inherently caused by the nature of the graphitization process [18,20]. In order

79  to overcome this limitation, laser-induced graphitization in diamond can be combined with a

80  preliminary MeV-ion-induced graphitization stage. By taking advantage of the high degree of

81  control on the geometrical properties (depth, thickness) of MeV-ion-induced buried graphitic

82  structures in diamond allowed by the peculiar nuclear energy loss profile of MeV ions [29], this

83  double-step procedure guarantees a better definition in the material micro-structuring [30] and

84  also represents an interesting improvement in the realization of particle detectors [26,31,32],

85  bolometers [33,34], bio-sensors [35–37], metallic-dielectric structures [38] and microfluidics

86  [39].

87  In the present paper we report on the use of ns-pulsed laser irradiation for the structural

88  modification and thickening of sub-superficial graphitic layers in diamond, which were realized

89  by means of MeV ion implantation. The above-mentioned structures are imaged before and after

90  the selective removal of the graphitic phase with respect to the surrounding diamond matrix, and

91  are characterized in their structural properties by transmission electron microscopy.

92

93  **2. Experimental**

94  In the present study, a commercial synthetic (001) single-crystal diamond grown by High

95  Pressure High Temperature method (HPHT) by ElementSix (Ascot, UK) was used. The diamond

96  is $3\times3\times0.3$ mm$^3$ in size and it is classified as type Ib, having a nominal substitutional nitrogen

97  concentration between 10 ppm and 100 ppm. The sample is cut along the 100 crystal direction

98  and it is optically polished on the two opposite large faces.

99  The sample was implanted at room temperature at the "Service Faisceaux d'Ions" laboratory of

100  the Nuclear Physics Institute (University of Claude Bernard Lyon 1) across one of the two main

101  polished surfaces with a broad 2 MeV He$^+$ ion beam to deliver a uniform fluence of $1\times10^{17}$ cm$^{-2}$

102  across the irradiated area. During the implantation, the beam current was ~200 Na. The process

103  of damage induced by MeV ions in matter occurs mainly at the end of ion range, where the cross

104  section for nuclear collisions is strongly enhanced, after the ion energy is progressively reduced

105  by electronic interactions occurring in the initial stages of the ion path [40]. Figure 1 shows the

106  strongly non-uniform depth profile of the density of induced vacancies (#$_{vac}$ cm$^{-3}$) evaluated in a

107  linear approximation as the product between the implantation fluence (#$_{ions}$ cm$^{-2}$) and the linear

108  density of induced vacancies per single ion (#$_{vac}$ cm$^{-1}$ #$_{ions}^{-1}$). The latter quantity was estimated

109  with the "Stopping and Range of Ions in Matter" (SRIM)-2013.00 Monte Carlo code [29] in

110  "Detailed calculation with full damage cascade" mode by taking an atom displacement energy

111  value of 50 Ev [41]. The high density of damage induced by ion implantation promotes the

112  conversion of the diamond lattice to an amorphous phase, which is located ~3.5 μm below the

113  sample surface.

114
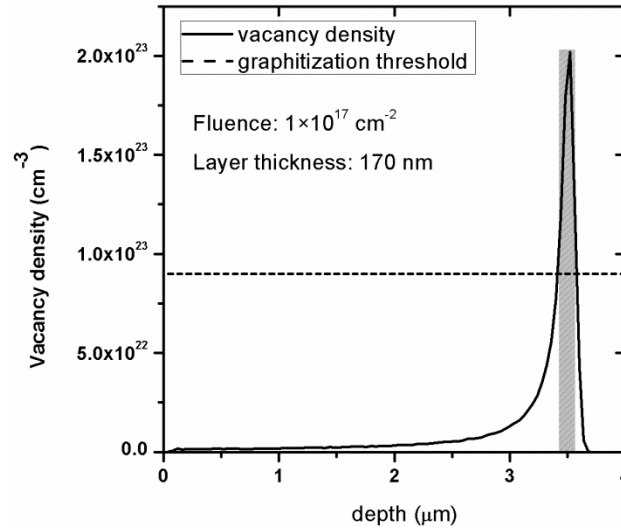
Fig. 1: Depth profile of the volumetric vacancy density induced in diamond by 2 MeV He[+] implanted at a fluence of $1 \times 10^{17}$ cm[-2]. The graphitization threshold is reported in dashed line. The amorphized region is highlighted by the grey area in correspondence of the intersection of the Bragg peak with the graphitization threshold.

118

The above-mentioned implantation fluence allowed to overcome a critical damage density, usually referred as "graphitization threshold" [42], whose value in the above-mentioned linear approximation has been estimated as $\sim 9 \times 10^{22}$ cm$^{-3}$ for light MeV irradiation [43], as indicated in Figure 1. Such a model of the damage profile has to be considered as a rough estimation since it results from a linearly cumulative effect of ion damage, i.e. by neglecting any damage saturation effects occurring at high damage levels such as self-annealing and vacancies interactions [44,45]. Nonetheless, in this context it can be considered as a satisfactory approach to estimate the depth and thickness of the buried region. After ion implantation, the sample was thermally annealed for 1 hour at a temperature of 900 °C, which is suitable for the conversion of amorphous carbon to a graphitic phase, as confirmed by TEM studies [46–48]. Concurrently, the annealing process restores the pristine diamond structure in the lightly-damaged cap layer, i.e. the region comprised

130  between the surface and the buried graphitic layer [49,50]. The process was carried out in

131  vacuum (p $\approx 10^{-6}$ mbar) to avoid accidental etching of the diamond surface due to oxidation.

132  The ion-implanted side of the sample was subsequently irradiated with nanosecond-pulsed

133  Nd:YAG laser (EzLaze3 by New Wave) equipped with a Q-switching system. This laser source

134  generates pulses of 4 ns duration with a repetition rate of either 1 Hz or 5 Hz. Two different

135  emission wavelengths can be selected, i.e. 1064 nm and 532 nm, the second one being obtained

136  by means of an angle-tuned KTP crystal. The laser beam is focused onto the sample with a

137  microscope supplied with 5×, 20× and 100× objective lenses. The co-axial imaging through the

138  microscope offers the opportunity of monitoring the sample processing in real time. Using the

139  532 nm wavelength and the 100× objective, the maximum emission power is 150 Kw and the

140  minimum size of the spot is 5×5 $\mu m^2$, thus resulting in a maximum power density of

141  ~22 GW $cm^{-2}$.

142  A Quanta 3D™ dual-beam system by FEI available at the "NanoFacility Piemonte" laboratories

143  of the INRiM Institute was employed to cross-section the sample by 30 keV $Ga^+$

144  focused-ion-beam (FIB) milling and to estimate the thickness of the graphitic layer before and

145  after the laser irradiation by SEM imaging .

146  The selective electrochemical etching of the graphite was performed with the purpose of

147  enhancing the topographical contrast in the SEM imaging of the buried layers. This process was

148  performed by immerging the sample in a water solution of $H_3BO_3$ ($4\times10^{-3}$ mol $l^{-1}$ concentration)

149  for 1 hour applying a DC voltage of 150–200 V through a couple of platinum electrodes placed

150  in close proximity of the sample [51].

151  The TEM imaging was performed at the Microscopy laboratories of the Bio21 Institute

152  (University of Melbourne) for a detailed study of the thickness and the structure of the graphitic

153    layers before and after laser annealing. To this scope, a Tecnai TF20 electron microscope

154    operated at 200 keV was employed. Cross-sectional TEM samples with thickness ~100 nm were

155    prepared in [110] and [100] orientations using a standard FIB lift-off technique. Selected area

156    diffraction (SAD) patterns were collected with smallest aperture (diameter ~180 nm in the

157    specimen plane). Nano-beam diffraction patterns were collected in nano-beam scanning TEM

158    (STEM) mode with beam size ~10 nm. Electron energy loss spectroscopy (EELS) was conducted

159    by employing a Gatan Enfina energy filter.

160

161    **3. Results and discussion**

162    FIB milling was employed to allow the cross-sectional SEM imaging of the ion-implanted and

163    subsequently annealed regions, as shown in Fig. 2a. The presence of the graphitic layer

164    embedded in the diamond matrix can be recognized in the dark grey horizontal strip, although

165    the low contrast in the secondary emission yield between graphite and diamond does not allow

166    performing an accurate measure of its thickness.

167    Selective etching of the graphite was therefore performed in order to improve imaging contrast

168    and facilitate the measurement of the thickness of the sub-superficial layer. Fig. 2b shows a SEM

169    micrograph of the same region of the sample reported in Fig. 2a, after selective chemical etching

170    of the graphite layer. The previously graphitized region now corresponds to a gap within the

171    material, thus allowing a better visibility of its thickness and depth.

172
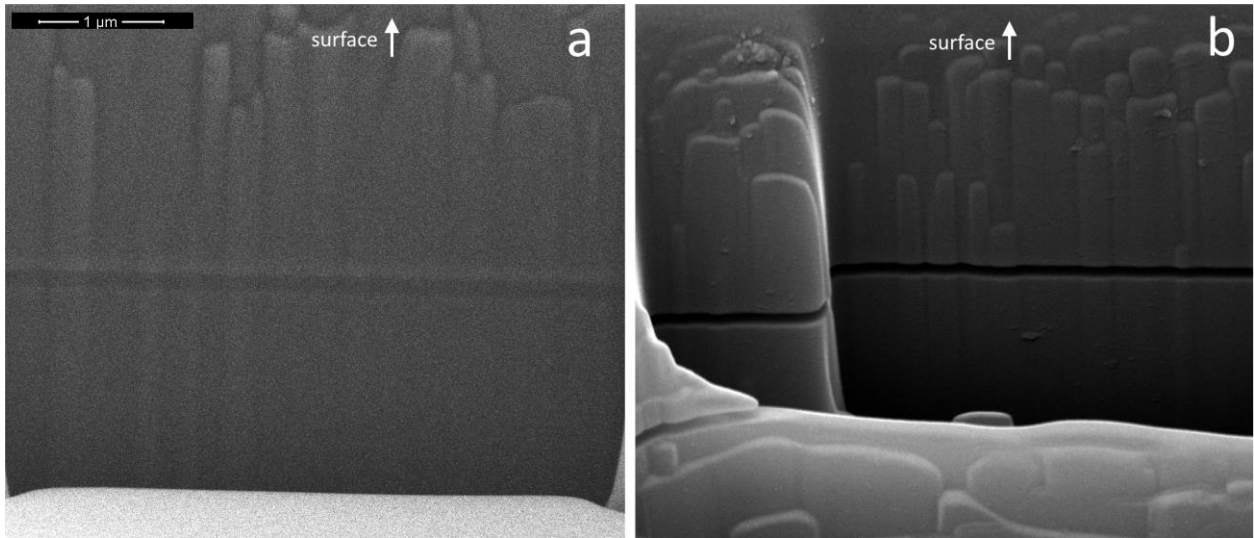
Fig. 2: Cross-sectional SEM micrographs of the sub-superficial graphitic layer in ion-implanted and annealed diamond a) before and b) after the selective etching process. A better definition of the geometrical parameters of the buried structure is clearly obtained after its selective removal by means of the etching process.

The thickness of the buried layer evaluated from Fig. 2a is $(200 \pm 40)$ nm, while it was estimated $(140 \pm 20)$ nm from Fig. 2b. This discrepancy is due to the relaxation of the upper cap layer, as it will be more extensively discussed in the following.

A more detailed structural characterization of the investigated regions was performed by means of cross-sectional TEM microscopy and EELS spectroscopy. A bright-field TEM micrograph and the corresponding Selected Area Diffraction (SAD) pattern of the implanted layer after thermal annealing are shown in Figs. 3a and 3b, respectively. The implanted layer is clearly visible due to the higher contrast and its width was estimated as $(130 \pm 3)$ nm. As shown in Fig. 3b, the diffraction pattern is characterized by well-defined spots arising from the diffraction of the bulk diamond, as well as arcs along the {220} reflections from the graphitic C-planes of the implanted layer. As shown in Fig. 3c, the corresponding EELS spectrum from the buried graphitic layer of the same region has a prominent feature at ~285 Ev, which is characteristic of

190  $sp^2$ bonding. Therefore, TEM diffraction pattern combined with EELS confirm the conversion of

191  the implanted layer into a nanocrystalline graphic phase with predominant orientation of

192  C-planes normal to the diamond surface.
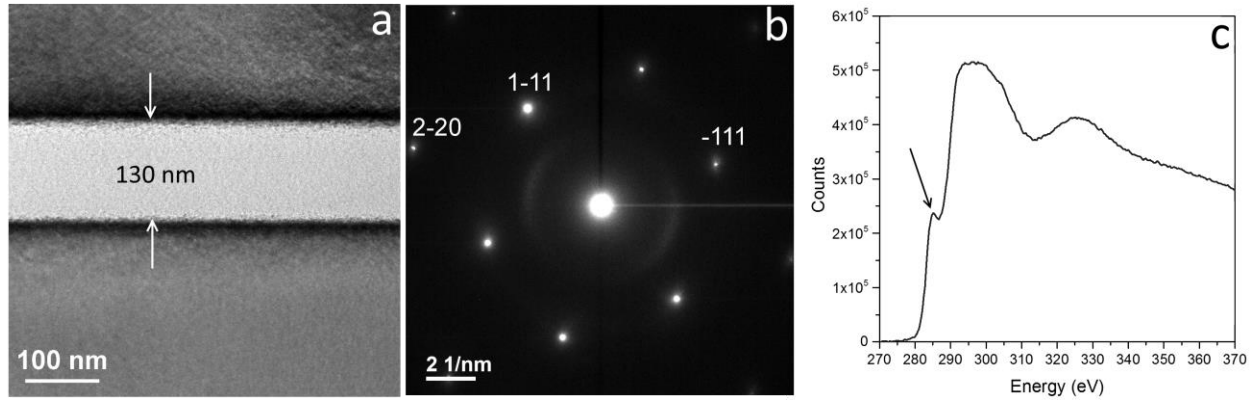
193



194  Fig. 3: a) Bright-field TEM cross-section micrograph of the sub-superficial graphitic layer in diamond before laser

195  irradiation (the sample surface is located towards the top of the picture). The thickness of the ion-implanted and

196  subsequently annealed structure is highlighted, corresponding to $(130 \pm 3)$ nm. B) SAD pattern taken from the same

197  area, showing well defined spots and arcs respectively from the diamond and graphitic regions. C) EELS spectrum

198  of the carbon K-edge taken from the implanted layer; the characteristic feature at 285 eV is indicated by the arrow.

199

200  Multiple-pulse laser irradiation at $\lambda = 532$ nm wavelength of the ion-implanted and subsequently

201  annealed diamond sample was carried out at two different powers densities (namely,

202  0.41 GW $cm^{-2}$ and 0.45 GW $cm^{-2}$) over an area of $26 \times 26$ $\mu m^2$.

203  Cross-sectional bright- and dark-field TEM micrographs of an area irradiated with 50 laser

204  pulses at a power density of 0.41 GW $cm^{-2}$ are reported in Figs. 4a and 4b, respectively, and

205  show a complex multi-layer structure within the buried layer. The laser-induced graphitic layer,

206  formed in the region located directly above the ion-implanted layer, results in an overall

207  thickness of $(690 \pm 15)$ nm. At the bottom of Fig. 4b (i.e. towards the bulk of the sample), the

208  nanocrystalline graphite layer due to ion implantation is clearly distinguishable, exhibiting the

209    same thickness measured before the laser irradiation (see Fig. 2) and no appreciable differences

210    in its structure.
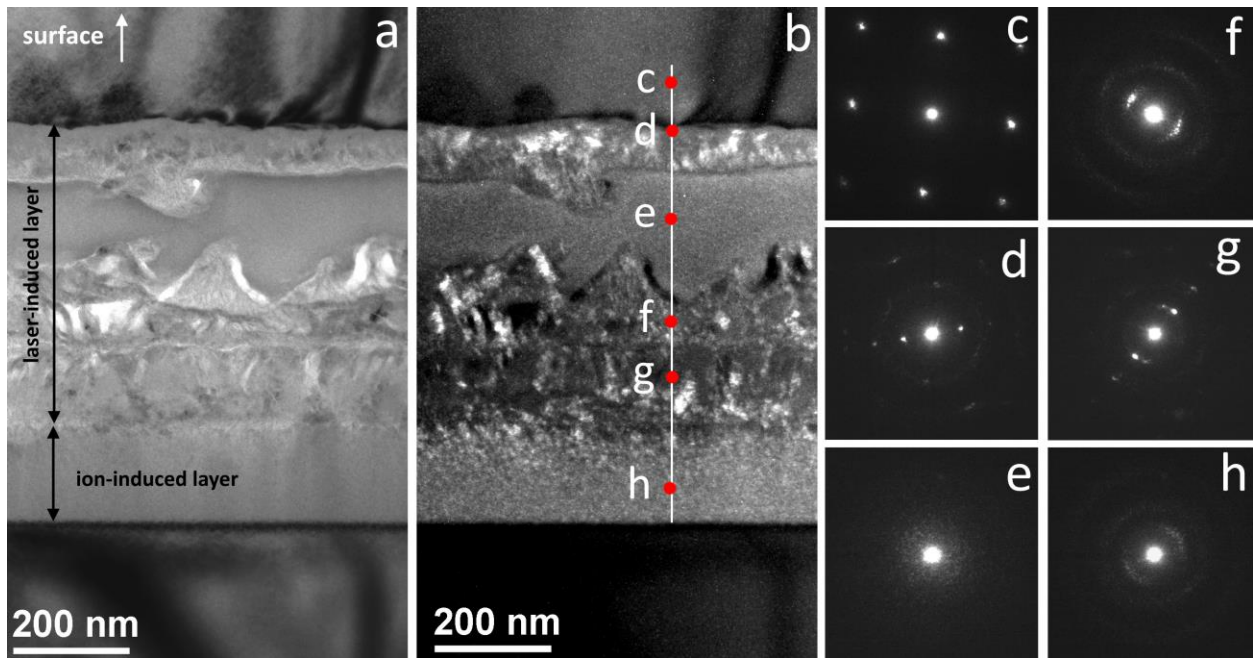


Fig. 4: a) Bright- and b) dark-field TEM cross section micrographs of a laser irradiated ($\lambda$ = 532 nm, power density:

0.41 GW cm$^{-2}$, 50 pulses) nanocrystalline graphitic sub-superficial layer obtained after annealing at 900 °C of an

implanted diamond region. The layer thickens towards the sample surface (i.e. towards the top of the figure), with a

complex structuring of the modified region consisting in amorphous-carbon and nanocrystalline-graphite layers. The

numbered red dots in b) highlight the regions from which the diffraction patterns reported in c-h) were acquired.

218    The laser-induced phase transition is driven by thermal effects that originate as a consequence of

219    the strong absorption of the laser radiation by the implanted graphitic layer. Since the laser beam

220    irradiates the side of the nanocrystalline graphitic layer facing the sample surface, the induced

221    heating of the material is mainly localized within the "cap layer" comprised between the layer

222    itself and the sample surface rather than towards the bulk, and therefore graphitization mainly

223    occurs in such direction. An estimate of the temperature rise in the cap layer can be obtained

224    from the pressure-temperature phase diagram of elemental carbon [52], with a similar approach

225   to what is reported in [2]. Finite element simulation studies from diamond samples implanted

226   under the same experimental conditions [53] indicate that the regions surrounding the buried

227   graphitic layer experience pressures of 8–10 GPa due to its constrained volume expansion.

228   Furthermore, the experimental evidence indicates that the temperature rise is high enough to

229   drive the graphitization process within the corresponding stable portion of the phase diagram,

230   without incurring in its liquefaction. The laser-induced local temperature rise is therefore

231   estimated between 2500 °C and 4500 °C. Such a significant heating is expected to rapidly

232   dissipate due to the high thermal conductivity of diamond.

233   Nano-beam diffraction patterns were taken in scanning TEM mode along the line shown in

234   Fig. 4b, which is crossing perpendicularly the graphitic layer at 10 nm steps. A selection of the

235   obtained diffraction patterns are shown in Figs. 4c-h. The peculiar structure of the laser-induced

236   layer is characterized by the presence of an amorphous carbon phase (diffraction pattern in

237   Fig. 4e) comprised between two polycrystalline graphitic phases (diffraction patterns in Figs. 4d

238   and 4f), as clearly visible in the dark-field micrograph of Fig. 4b. The dark field micrograph was

239   constructed by selecting the graphitic arcs in the diffraction pattern, and therefore the graphitic

240   crystals appear as bright spots in it. These spots have <5 nm sizes in implanted layer and much

241   larger dimensions in the laser-induced layer. The observed multi-layer structure is somewhat

242   surprising and can be qualitatively attributed to a complex combination of thermal gradient and

243   stress effects occurring in the diamond during the pulsed laser irradiation [54].
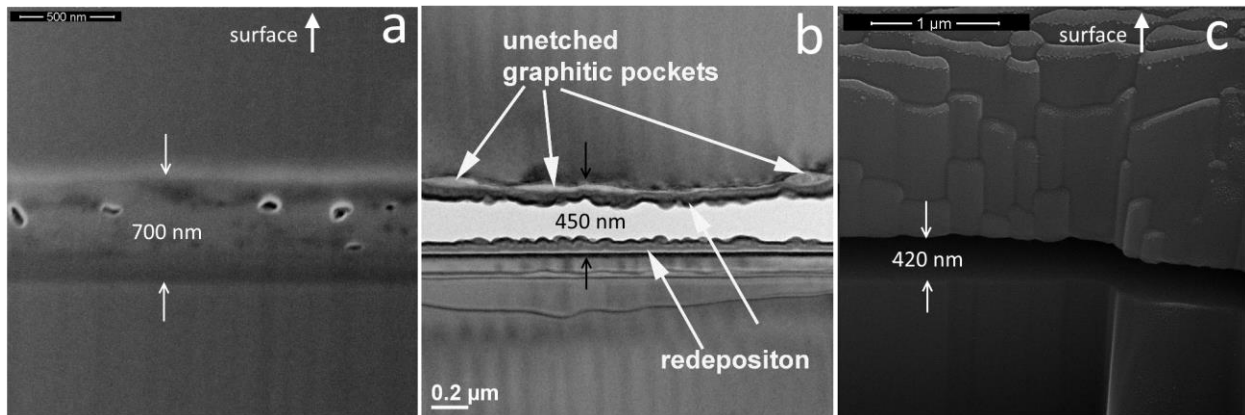
244   A SEM micrograph of the same laser-irradiated region is reported in Fig. 5a, from which a layer

245   thickness of $(700 \pm 70)$ nm can be estimated, compatibly (although with lower accuracy) with

246   what obtained from TEM imaging. The amorphous areas are visible inside the graphitic layer, as

247    well as some voids. These voids were probably filled with re-deposited material during TEM

248    sample preparation and are therefore not visible in TEM images reported in Figs. 4a and 4b.

249    Following the same procedure adopted for the sample after implantation and annealing (see

250    Fig. 2), a selective electrochemical etching was carried out and the resulting structure is shown in

251    the TEM micrograph reported in Fig. 5b. The removal of the graphitic layer is evident in both

252    micrographs. Also, re-deposited material is visible on both surfaces of the gap, as commonly

253    observed in FIB milling. As shown in Fig. 5b, after laser irradiation and chemical etching the

254    buried layer was not entirely removed, but rather only the ion-induced nanocrystalline graphite

255    layer was etched, as confirmed by the comparison of the thicknesses of the regions reported in

256    Figs. 4a and 5b. This is a surprising result, since the polycrystalline graphitic phase formed

257    during laser irradiation is expected to be effectively etched by the electrochemical attack.

258    A thermal treatment at 900 °C for 2 hours was therefore performed on the same sample after

259    laser irradiation, with the purpose of inducing the graphitization of residual amorphous/distorted

260    material in the un-etched region. Afterwards, the sample was exposed to the same etching

261    process. As shown in Fig. 5c, the width of the etched layer in the laser-irradiated and annealed

262    sample increased up to $(420 \pm 20)$ nm, indicating a full removal of the laser-irradiated layer. As

263    already reported for the sample before laser irradiation, a discrepancy between the thickness

264    values of the laser-induced layer and the remaining gap is observed (see Figs. 5a and 5c). As

265    mentioned before, this effect can be explained by considering that a relaxation of the diamond

266    cap layer takes place after the removal of the graphitic layer. Since the graphite is characterized

267    by a significantly lower atomic density with respect to diamond, a volume expansion takes place

268    upon the graphitization process [55,56], thus deforming the upper diamond cap layer comprised

269     between the graphic layer and the sample surface. Once the graphite is removed, the cap layer

270     undergoes a structural relaxation which induces the thinning of the etched region.

271



272     Fig. 5: a) Cross sectional SEM micrograph of the buried damaged layer after laser irradiation ($\lambda$ = 532 nm, power

273     density: 0.41 GW cm$^{-2}$, 50 pulses). b) Cross-sectional TEM micrograph of the same layer reported in a) after

274     electrochemical etching; together with the characteristic re-deposited material present in the gap, un-etched

275     laser-induced layers are recognizable around the gap. c) Cross-sectional SEM micrograph of the same layer reported

276     in a) after a further 900 °C annealing step and electrochemical etching; no un-etched layers are visible.

277

278     Even more surprisingly, after the first etching process (i.e. before the second annealing step)

279     highly oriented graphitic clusters were found in correspondence of the partially un-etched

280     diamond/graphite interface which was closest to the sample surface, as shown in Fig. 5b.

281     Fig. 6a reports a high-resolution TEM micrograph of one of these clusters. The presence of

282     graphite C-planes is clearly visible in the corresponding diffraction pattern reported in Fig. 6c,

283     indicating the highly oriented structure of these graphitic clusters.

284
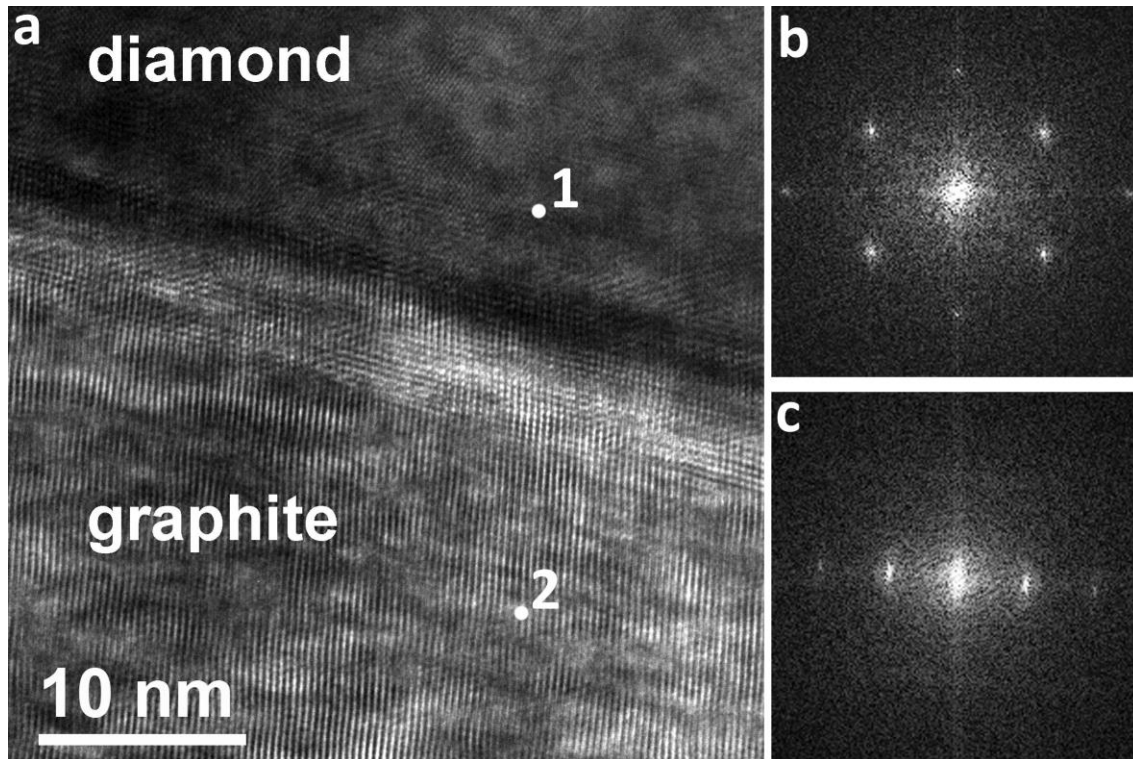
Fig. 6. a) High resolution TEM micrograph of one of the highly oriented graphitic clusters remaining near the diamond interface after the chemical etching of the laser-irradiated sample. The corresponding diffraction patterns from diamond (spot "1") and graphite (spot "2") are reported in b) and c), respectively.

The results reported so far refer to regions of the sample which were exposed to 50 laser pulses and subsequently subjected to different annealing and/or etching processes. A systematic investigation of the laser-induced graphitization was also carried out as a function of the laser irradiation parameters (power, number of pulses). As previously reported, the implanted and subsequently annealed sample was irradiated with 532 nm laser pulses and power densities of $0.41\ \mathrm{GW\ cm^{-2}}$ and $0.45\ \mathrm{GW\ cm^{-2}}$ over different $26{\times}26\ \mathrm{\mu m^2}$ areas. Following these laser irradiations, the sample was annealed at 900 °C for 2 hours with the purpose of inducing a full graphitization in the irradiated areas, consistently with the above-mentioned results. Also in this case, cross-sectional SEM imaging of the irradiated regions was systematically performed to

299 evaluate the thickening in regions processed with different laser irradiation conditions, and the

300 layer thicknesses were measured before and after the etching process.

301 Fig. 7 summarizes the results obtained for the two different power densities for a number of laser

302 pulses ranging between 1 and 300. It is evident that the thickness of the graphitic sub-superficial

303 layer obtained after laser irradiation and thermal annealing increases at increasing numbers of

304 laser pulses, up to more than 6 times its initial value. The trends reported in Fig. 7 clearly

305 indicate a strong sub-linear dependence of the layer thickness from the number of laser pulses. It

306 is also evident that the power density has a direct influence on the thickening process, with the

307 larger power density determining a more pronounced thickening for the same number of laser

308 pulses. A maximum total thickness of ~1.25 μm was achieved, with the process being limited by

309 the large mechanical stresses that build up in the diamond cap layer which ultimately cause local

310 mechanical fractures. For this reason, power densities and number of pulses larger than the ones

311 shown in Fig. 7 could not be tested without incurring in structural damage effects. Consistently

312 with what was previously observed, for all of the structures the second annealing step resulted in

313 a complete removal of the buried graphitic layers upon electrochemical etching. It is also worth

314 stressing that, as explained above, the thickness of the gaps obtained after selective

315 electrochemical etching is systematically smaller than the thickness of the laser-induced

316 graphitic layers, as shown in Fig 7.
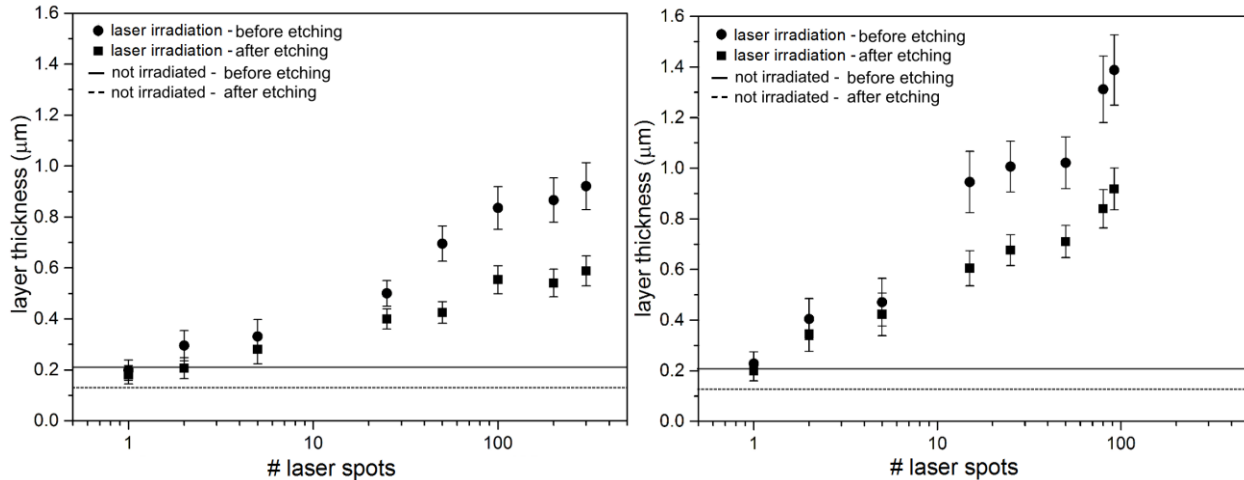
317

318  Fig. 7: Plot of the measured thickness of the sub-superficial graphitic layers versus the number of $\lambda = 532$ nm laser

319  pulses for two different power densities, i.e. a) $P = 0.41$ GW cm$^{-2}$ and b) $P = 0.45$ GW cm$^{-2}$. The thickness

320  measurements are reported both before (circular dots) and after (square dots) the selective etching process. Likewise,

321  the horizontal lines indicate the thicknesses of the pristine ion-induced layer, both before (continuous line) and after

322  (dashed line) the selective etching process.

323

## 4. Conclusions

325  We reported on the effect of ns-pulsed $\lambda = 532$ nm laser irradiation on the thickening of

326  sub-superficial graphitic layers in diamond obtained by means of 2 MeV He$^+$ ion implantation

327  and subsequent high-temperature annealing. Cross-sectional TEM and EELS measurements

328  elucidated the complex structuring of the processed regions into amorphous and nanocrystalline

329  graphitic multi-layers. The complete conversion of the laser-induced layers to an etchable

330  graphitic phase was obtained only upon thermal annealing at 900 °C, while a highly-oriented

331  phase was found in the residual graphitic pockets after selective etching of the non-annealed

332  samples. A systematic SEM investigation of the thickening of the graphitic region was carried

333  out as a function of the laser irradiation parameters (power density, number of pulses). An

334    increase up to 650% of the initial layer thickness was reached without incurring into critical

335    mechanical failures due to induced mechanical stresses.

336    By allowing a fine tuning of geometrical and structural properties of graphitic layers formed by

337    ion irradiation, laser-induced graphitization offers interesting opportunities for a new level of

338    control in the fabrication of buried graphitic structures in diamond, with appealing applications

339    in different fields in which MeV ion beam lithography and laser graphitization were successfully

340    employed [26,31–36,38,39]

341

350

351 **References**

352

353 [1] R.J. Nemanich, J. a. Carlisle, A. Hirata, K. Haenen, CVD diamond—Research,
354 applications, and challenges, MRS Bull. 39 (2014) 490–494. doi:10.1557/mrs.2014.97.

355

356 [2] S. Prawer, D.N. Jamieson, R. Kalish, Investigation of carbon near the graphite-diamond-
357 liquid triple point, Phys. Rev. Lett. 69 (1992) 2991–2994.
358 doi:10.1103/PhysRevLett.69.2991.

359

360 [3] S. Prawer, Ion implantation of diamond and diamond films, Diam. Relat. Mater. 4 (1995)
361 862–872. doi:10.1016/0925-9635(94)05263-8.

362

363 [4] R. Kalish, a. Reznik, K.W. Nugent, S. Prawer, The nature of damage in ion-implanted
364 and annealed diamond, Nucl. Instruments Methods Phys. Res. Sect. B Beam Interact. with
365 Mater. Atoms. 148 (1999) 626–633. doi:10.1016/S0168-583X(98)00857-X.

366

367 [5] R. Kalish, S. Prawer, Graphitization of diamond by ion impact: Fundamentals and
368 applications, Nucl. Instruments Methods Phys. Res. Sect. B Beam Interact. with Mater.
369 Atoms. 106 (1995) 492–499. doi:10.1016/0168-583X(95)00758-X.

370

371 [6] A.A. Gippius, R.A. Khmelnitskiy, V.A. Dravin, S.D. Tkachenko, Formation and
372 characterization of graphitized layers in ion-implanted diamond, Diam. Relat. Mater. 8
373 (1999) 1631–1634. doi:10.1016/S0925-9635(99)00047-3.

374

375 [7] F. Picollo, P. Olivero, F. Bellotti, Ž. Pastuović, N. Skukan, A. Lo Giudice, et al.,
376 Formation of buried conductive micro-channels in single crystal diamond with MeV C
377 and He implantation, Diam. Relat. Mater. 19 (2010) 466–469.
378 doi:10.1016/j.diamond.2010.01.005.

379

380 [8] F. Picollo, D. Gatto Monticone, P. Olivero, B. a. Fairchild, S. Rubanov, S. Prawer, et al.,
381 Fabrication and electrical characterization of three-dimensional graphitic microchannels in
382 single crystal diamond, New J. Phys. 14 (2012) 053011. doi:10.1088/1367-
383 2630/14/5/053011.

384

385 [9] V.N. Strekalov, V.I. Konov, V. V. Kononenko, S.M. Pimenov, Early stages of laser
386 graphitization of diamond, Appl. Phys. A Mater. Sci. Process. 76 (2003) 603–607.
387 doi:10.1007/s00339-002-2014-3.
388

389 [10] T. V. Kononenko, M.S. Komlenok, V.P. Pashinin, S.M. Pimenov, V.I. Konov, M. Neff, et
390 al., Femtosecond laser microstructuring in the bulk of diamond, Diam. Relat. Mater. 18
391 (2009) 196–199. doi:10.1016/j.diamond.2008.07.014.
392

393 [11] V.N. Strekalov, Graphitization of diamond stimulated by electron-hole recombination,
394 Appl. Phys. A Mater. Sci. Process. 80 (2005) 1061–1066. doi:10.1007/s00339-003-2362-
395 7.
396

397 [12] H. Jeschke, M. Garcia, K. Bennemann, Microscopic analysis of the laser-induced
398 femtosecond graphitization of diamond, Phys. Rev. B. 60 (1999) R3701–R3704.
399 doi:10.1103/PhysRevB.60.R3701.
400

401 [13] K.H. Bennemann, Photoinduced phase transitions., J. Phys. Condens. Matter. 23 (2011)
402 073202. doi:10.1088/0953-8984/23/7/073202.
403

404 [14] M. Rothschild, Excimer-laser etching of diamond and hard carbon films by direct writing
405 and optical projection, J. Vac. Sci. Technol. B Microelectron. Nanom. Struct. 4 (1986)
406 310. doi:10.1116/1.583320.
407

408 [15] E. Alemanno, a. P. Caricato, G. Chiodini, M. Martino, P.M. Ossi, S. Spagnolo, et al.,
409 Excimer laser-induced diamond graphitization for high-energy nuclear applications, Appl.
410 Phys. B Lasers Opt. 113 (2013) 373–378. doi:10.1007/s00340-013-5487-1.
411

412 [16] C.Z. Wang, K.M. Ho, M.D. Shirk, P. a. Molian, Laser-induced graphitization on a
413 diamond (111) surface, Phys. Rev. Lett. 85 (2000) 4092–4095.
414 doi:10.1103/PhysRevLett.85.4092.
415

416 [17] Y. Shimotsuma, Three-dimensional Nanostructuring of Transparent Materials by the
417 Femtosecond Laser Irradiation, J. Laser Micro/Nanoengineering. 1 (2006) 181–184.
418 doi:10.2961/jlmn.2006.03.0006.
419

420 [18] T. V. Kononenko, V.I. Konov, S.M. Pimenov, N.M. Rossukanyi, a. I. Rukovishnikov, V.
421 Romano, Three-dimensional laser writing in diamond bulk, Diam. Relat. Mater. 20 (2011)
422 264–268. doi:10.1016/j.diamond.2010.12.013.
423

424 [19] S.M. Pimenov, B. Neuenschwander, B. Jäggi, V. Romano, Effect of crystal orientation on
425 picosecond-laser bulk microstructuring and Raman lasing in diamond, Appl. Phys. A
426 Mater. Sci. Process. 114 (2014) 1309–1319. doi:10.1007/s00339-013-7953-3.
427

428    [20]   S.M. Pimenov, I.I. Vlasov, A. a. Khomich, B. Neuenschwander, M. Muralt, V. Romano,
429          Picosecond-laser-induced structural modifications in the bulk of single-crystal diamond,
430          Appl. Phys. A Mater. Sci. Process. 105 (2011) 673–677. doi:10.1007/s00339-011-6645-0.
431

432    [21]   R.D. Simmonds, P.S. Salter, A. Jesacher, M.J. Booth, Three dimensional laser
433          microfabrication in diamond using a dual adaptive optics system, Opt. Express. 19 (2011)
434          24122. doi:10.1364/OE.19.024122.
435

436    [22]   B. Sun, P.S. Salter, M.J. Booth, High conductivity micro-wires in diamond following
437          arbitrary paths, Appl. Phys. Lett. 105 (2014) 231105. doi:10.1063/1.4902998.
438

439    [23]   S. Lagomarsino, M. Bellini, C. Corsi, F. Gorelli, G. Parrini, M. Santoro, et al., Three-
440          dimensional diamond detectors: Charge collection efficiency of graphitic electrodes, Appl.
441          Phys. Lett. 103 (2013) 233507. doi:10.1063/1.4839555.
442

443    [24]   M. Pacilli, P. Allegrini, G. Conte, E. Spiriti, V.G. Ralchenko, M. Komlenok, et al., Beta
444          particles sensitivity of an all-carbon detector, Nucl. Instruments Methods Phys. Res. Sect.
445          A   Accel.   Spectrometers,   Detect.   Assoc.   Equip.   738   (2014)   119–125.
446          doi:10.1016/j.nima.2013.12.022.
447

448    [25]   E. Alemanno, M. Martino,  a. P. Caricato, M. Corrado, C. Pinto, S. Spagnolo, et al., Laser
449          induced nano-graphite electrical contacts on synthetic polycrystalline CVD diamond for
450          nuclear   radiation   detection,   Diam.   Relat.   Mater.   38   (2013)   32–35.
451          doi:10.1016/j.diamond.2013.06.006.
452

453    [26]   S. Lagomarsino, M. Bellini, C. Corsi, S. Fanetti, F. Gorelli, I. Liontos, et al., Electrical
454          and Raman-imaging characterization of laser-made electrodes for 3D diamond detectors,
455          Diam. Relat. Mater. 43 (2014) 23–28. doi:10.1016/j.diamond.2014.01.002.
456

457    [27]   A. Oh, B. Caylar, M. Pomorski, T. Wengler, A novel detector with graphitic electrodes in
458          CVD diamond, Diam. Relat. Mater. 38 (2013) 9–13. doi:10.1016/j.diamond.2013.06.003.
459

460    [28]   S. Su, J. Li, G.C.B. Lee, K. Sugden, D. Webb, H. Ye, Femtosecond laser-induced
461          microstructures on diamond for microfluidic sensing device applications, Appl. Phys. Lett.
462          102 (2013) 231913. doi:10.1063/1.4811170.
463

464    [29]   J.F. Ziegler, M.D. Ziegler, J.P. Biersack, SRIM - The stopping and range of ions in matter
465          (2010), Nucl. Instruments Methods Phys. Res. Sect. B Beam Interact. with Mater. Atoms.
466          268 (2010) 1818–1823. doi:10.1016/j.nimb.2010.02.091.
467

468    [30]    V. V. Kononenko, S.M. Pimenov, T. V. Kononenko, V.I. Konov, P. Fischer, V. Romano,
469            et al., Laser-induced phase transitions in ion-implanted diamond, Diam. Relat. Mater. 12
470            (2003) 277–282. doi:10.1016/S0925-9635(03)00063-3.
471

472    [31]    B. Caylar, M. Pomorski, P. Bergonzo, Laser-processed three dimensional graphitic
473            electrodes for diamond radiation detectors, Appl. Phys. Lett. 103 (2013) 043504.
474            doi:10.1063/1.4816328.
475

476    [32]    J. Forneris, V. Grilj, M. Jakšić,  a. Lo Giudice, P. Olivero, F. Picollo, et al., IBIC
477            characterization of an ion-beam-micromachined multi-electrode diamond detector, Nucl.
478            Instruments Methods Phys. Res. Sect. B Beam Interact. with Mater. Atoms. 306 (2013)
479            181–185. doi:10.1016/j.nimb.2012.12.056.
480

481    [33]    A.Y. Klokov, A.I. Sharkov, T.I. Galkina, R.A. Khmel'nitskii, V.A. Dravin, A.A. Gippius,
482            A bolometric detector built into the diamond bulk, Tech. Phys. Lett. 27 (2001) 581–582.
483            doi:10.1134/1.1388950.
484

485    [34]    A.Y. Klokov, A.I. Sharkov, T.I. Galkina, R.A. Khmelnitsky, V.A. Dravin, V.G.
486            Ralchenko, et al., Fast bolometric sensor built-in into polycrystalline CVD diamond, J.
487            Phys. Conf. Ser. 92 (2007) 012181. doi:10.1088/1742-6596/92/1/012181.
488

489    [35]    F. Picollo, S. Gosso, E. Vittone, A. Pasquarelli, E. Carbone, P. Olivero, et al., A new
490            diamond biosensor with integrated graphitic microchannels for detecting quantal exocytic
491            events   from   chromaffin   cells,   Adv.   Mater.   25   (2013)   4696–4700.
492            doi:10.1002/adma.201300710.
493

494    [36]    F. Picollo, A. Battiato, E. Carbone, L. Croin, E. Enrico, J. Forneris, et al., Development
495            and Characterization of a Diamond-Insulated Graphitic Multi Electrode Array Realized
496            with Ion Beam Lithography, Sensors. 15 (2014) 515–528. doi:10.3390/s150100515.
497

498    [37]    F. Picollo,  a. Battiato, E. Bernardi, L. Boarino, E. Enrico, J. Forneris, et al., Realization of
499            a diamond based high density multi electrode array by means of Deep Ion Beam
500            Lithography, Nucl. Instruments Methods Phys. Res. Sect. B Beam Interact. with Mater.
501            Atoms. (2015). doi:10.1016/j.nimb.2014.11.119.
502

503    [38]    M. Shimizu, Y. Shimotsuma, M. Sakakura, T. Yuasa, H. Homma, Y. Minowa, et al.,
504            Periodic metallo-dielectric structure in diamond., Opt. Express. 17 (2009) 46–54.
505            doi:10.1364/OE.17.000046.
506

507    [39]    M. a. Strack, B. a. Fairchild, A.D.C. Alves, P. Senn, B.C. Gibson, S. Prawer, et al., Buried

picolitre fluidic channels in single-crystal diamond, 8923 (2013) 89232X. doi:10.1117/12.2035099.

[40] K.M. Knowles, Materials Analysis using a Nuclear Microprobe, J. Microsc. 189 (1998) 99–100. doi:10.1046/j.1365-2818.1998.0270c.x.

[41] D. Saada, J. Adler, R. Kalish, Transformation of diamond (sp(3)) to graphite (sp(2)) bonds by ion-impact, Int. J. Mod. Phys. C. 9 (1998) 61–69. http://www.worldscientific.com/doi/pdf/10.1142/S0129183198000066 (accessed October 24, 2013).

[42] C. Uzan-Saguy, V. Richter, S. Prawer, Y. Lifshitz, E. Grossman, R. Kalish, Nature of damage in diamond implanted at low temperatures, Diam. Relat. Mater. 4 (1995) 569–574. doi:10.1016/0925-9635(94)05290-5.

[43] P. Olivero, S. Rubanov, P. Reichart, B.C. Gibson, S.T. Huntington, J.R. Rabeau, et al., Characterization of three-dimensional microstructures in single-crystal diamond, Diam. Relat. Mater. 15 (2006) 1614–1621. doi:10.1016/j.diamond.2006.01.018.

[44] F. Bosia, S. Calusi, L. Giuntini, S. Lagomarsino, A. Lo Giudice, M. Massi, et al., Finite element analysis of ion-implanted diamond surface swelling, Nucl. Instruments Methods Phys. Res. Sect. B Beam Interact. with Mater. Atoms. 268 (2010) 2991–2995. doi:10.1016/j.nimb.2010.05.025.

[45] F. Bosia, N. Argiolas, M. Bazzan, B. a Fairchild, a D. Greentree, D.W.M. Lau, et al., Direct measurement and modelling of internal strains in ion-implanted diamond., J. Phys. Condens. Matter. 25 (2013) 385403. doi:10.1088/0953-8984/25/38/385403.

[46] D.P. Hickey, K.S. Jones, R.G. Elliman, Amorphization and graphitization of single-crystal diamond - A transmission electron microscopy study, Diam. Relat. Mater. 18 (2009) 1353–1359. doi:10.1016/j.diamond.2009.08.012.

[47] T.E. Derry, E.K. Nshingabigwi, M. Levitt, J. Neethling, S.R. Naidoo, Cross-section transmission electron microscopy of the ion implantation damage in annealed diamond, Nucl. Instruments Methods Phys. Res. Sect. B Beam Interact. with Mater. Atoms. 267 (2009) 2705–2707. doi:10.1016/j.nimb.2009.05.032.

[48] S. Rubanov, B. a. Fairchild, a. Suvorova, P. Olivero, S. Prawer, Structural transformation of implanted diamond layers during high temperature annealing, Nucl. Instruments Methods Phys. Res. Sect. B Beam Interact. with Mater. Atoms. (2015).

548  doi:10.1016/j.nimb.2015.07.020.
549

550 [49] P.F. Lai, S. Prawer, L. a. Bursill, Recovery of diamond after irradiation at high energy and
551      annealing, Diam. Relat. Mater. 10 (2001) 82–86. doi:10.1016/S0925-9635(00)00406-4.
552

553 [50] V.S. Drumm, A.D.C. Alves, B.A. Fairchild, K. Ganesan, J.C. McCallum, D.N. Jamieson,
554      et al., Surface damage on diamond membranes fabricated by ion implantation and lift-off,
555      Appl. Phys. Lett. 98 (2011) 231904. doi:10.1063/1.3597223.
556

557 [51] J.B. Posthill, D.P. Malta, T.P. Humphreys, G.C. Hudson, R.E. Thomas, R.A. Rudder, et
558      al., Method of fabricating a free-standing diamond single crystal using growth from the
559      vapor phase, J. Appl. Phys. 79 (1996) 2722. doi:10.1063/1.361144.
560

561 [52] F.P. Bundy, Pressure-temperature phase diagram of elemental carbon, Phys. A Stat. Mech.
562      Its Appl. 156 (1989) 169–178. doi:10.1016/0378-4371(89)90115-5.
563

564 [53] P. Olivero, F. Bosia, B. a. Fairchild, B.C. Gibson, a. D. Greentree, P. Spizzirri, et al.,
565      Splitting of photoluminescent emission from nitrogen-vacancy centers in diamond
566      induced by ion-damage-induced stress, New J. Phys. 15 (2013). doi:10.1088/1367-
567      2630/15/4/043027.
568

569 [54] T. V. Kononenko, a. a. Khomich, V.I. Konov, Peculiarities of laser-induced material
570      transformation inside diamond bulk, Diam. Relat. Mater. 37 (2013) 50–54.
571      doi:10.1016/j.diamond.2013.04.010.
572

573 [55] J.F. Prins, T.E. Derry, J.P.F. Sellschop, Volume expansion of diamond during ion
574      implantation at low temperatures, Nucl. Instruments Methods Phys. Res. Sect. B Beam
575      Interact. with Mater. Atoms. 18 (1986) 261–263. doi:10.1016/S0168-583X(86)80041-6.
576

577 [56] M. Piccardo, F. Bosia, P. Olivero, N. Pugno, An analytical model for the mechanical
578      deformation of locally graphitized diamond, Diam. Relat. Mater. 48 (2014) 73–81.
579      doi:10.1016/j.diamond.2014.07.006.
580